International Journal of Structural Stability and Dynamics
(2021) 2150120 (24 pages)

DOI: 10.1142/S0219455421501200

Artificial Intelligence-Based Prediction Models for Optimal Design of Tuned Mass Dampers in Damped Structures Subjected to Different Excitations

Sadegh Etedali[*,§], Zohreh Khosravi Bijaem[†], Nader Mollayi[‡]
and Vahide Babaiyan[‡]

[*]*Department of Civil Engineering*
Birjand University of Technology
P.O. Box 97175-569, Birjand, Iran

[†]*Department of Civil Engineering*
Hormozan Institute of Higher Education, Birjand, Iran

[‡]*Department of Computer Engineering*
Birjand University of Technology, Birjand, Iran
[§]*Etedali@birjandut.ac.ir*

Received 2 January 2021
Accepted 18 March 2021
Published 23 April 2021

Tuned mass damper (TMD) is a type of energy absorbers that can mitigate the vibrations of the main system if its frequency and damping ratios are well adjusted. By adopting simple assumptions on the structure and loadings, many analytical and empirical relationships have been presented for the estimation of the parameters for TMDs. In this research, methods based on the artificial intelligence (AI) techniques are proposed for optimal tuning of the TMD parameters of the main damped-structure for three kinds of loadings: white-noise base acceleration, external white-noise force, and harmonic base acceleration. For this purpose, a dataset using the cuckoo search (CS) optimization algorithm is created. The performance of the proposed methods based on the radial basis function (RBF) neural network, feed-forward neural network (FFNN), adaptive neuro-fuzzy inference system (ANFIS), and random forest (RF) techniques are evaluated by some statistical indicators. The results show the proper performance of these methods for the optimal estimation of the TMD parameters. Overall, the ANFIS method results in best matching with the observed dataset. Moreover, the simulation results indicate that the TMD's optimal frequency ratio is reduced, while its optimal damping ratio is increased, against the increase in the TMD mass ratio of the main structure subjected to harmonic base acceleration. This trend with a less slope is observed for the optimal frequency ratio of the TMD in the main structure subjected to external white-noise force; however, the optimal damping ratio of the TMD is independent of its mass ratio in this case. Similar results are obtained for the main structure subjected to white-noise base acceleration.

Keywords: Tuned mass damper; optimal design; radial basis function; neural network; neuro-fuzzy inference system; random forest.

[§]Corresponding author.

1. Introduction

Tuned mass damper (TMD) is one of the vibration control devices in mechanical and structural systems. It is widely utilized for the mitigation of vibration effects due to wind, wave, earthquake, impact, etc. The application areas of TMD are very wide; to mitigate the periodic resonance in vehicles like an airplane, a ship, and railway vehicles; the destructive effects of vibrations on the mechanical system; the undesirable vibrations of bridges and structures during wind and earthquake. Adjusting the TMD parameters has an important role in its efficacy for the mitigation of undesirable vibrations. Considering simple assumptions on the main structure and loading, the optimal design of TMD parameters is addressed by some researchers. Some closed-form expressions have been proposed.[1–4] Some researchers also confirmed that converting a multi-degree-of-freedom (MDOF) structure to an equivalent single-degree-of-freedom (SDOF) structure is possible and correct for the elastic structures with TMD.[5,6] Colherinhas *et al.*[7] studied on the optimal parameters of a pendulum TMD (PTMD) for controlling the vibrations of slender towers modeled as an SDOF mass-spring system subjected to an external random force. Some studies have been focused on the enhancement methods of the conventional TMD performance via a combination of the friction mechanism with TMD,[8] a novel bidirectional pounding tuned mass damper,[9] simultaneous use of base isolation system and TMD,[10] TMD fabricated using the Reid damping,[11] active TMD (ATMD) by adding a mechanism for applying the control force to TMD,[12,13] a combination of semi-active magneto-rheological (MR) damper with passive TMD,[14,15] the combination of piezoelectric friction damper as a semi-active device with TMD.[16] Nevertheless, the advantages of conventional TMD in terms of simplicity, low cost, and no need for external power have caused the study on TMD to be still interesting and ongoing. Besides, the application of the TMD is still ongoing for seismic application in buildings and bridges. Sufficiently realistic tuning of the TMD cannot be obtained via classical calculation methods. Hence, metaheuristic methods have recently been utilized for optimal tuning of TMD parameters. Some metaheuristic methods applied for optimal tuning of TMD parameters include genetic algorithms,[17–20] Min. Max. optimization procedure,[21] particle swarm optimization,[22,23] harmony search algorithm,[24] hybrid genetic-simulated annealing,[25] cuckoo search,[26,27] chaotic optimization algorithm,[28] and teaching-learning based optimization.[29]

The utilization of the metaheuristic methods is an iteration process that demands numerous numerical analyses. This is a time-consuming and boring process. AI techniques have been taken into account for overcoming the issue in engineering applications. AI is a branch of computer science that tries to design a system that could reactions similar behavior of a human, such as understanding complex situations, simulation of thought processes and modes of human reasoning and successful response to them, learning, and the ability to acquire knowledge and reasoning to solve problems. The most important branches of this knowledge are neural networks, fuzzy reasoning systems, and mechanic learning. In the techniques, a process of training of dataset is applied to build up a model of the system to aim at the prediction of the cases that have not yet been observed. AI techniques and machine learning have widely applied to various fields of engineering applications, such as mechanical engineering,[30] industrial engineering,[31] civil engineering,[32] computer engineering,[33] electrical engineering,[34] aerospace engineering,[35] chemical engineering[36] and medical engineering.[37]

TMD performance directly depends on adjusting the TMD parameters. The simplicity of tuning and accuracy of estimation of the optimal TMD parameters are important factors for the utilization of a method for this purpose. The use of meta-heuristic optimization algorithms for optimal tuning of the TMD parameters is a very time-consuming task due to the search of optimal parameters in a possible search space and the need for numerous numerical analyses of the motion equation. In engineering applications, presentation surrogate models created by AI and machinic learning techniques is an interesting topic to overcome the issue of computational costs in design processes using meta-heuristic optimization algorithms. The studied on the application of these techniques for the optimal design problem of the TMD parameters are limited in the literature. Etedali and Mollayi[38] proposed models based on least squares support vector machine models for the optimum design issue of the TMD parameters. Yücel *et al.*[39] utilized machine learning for the estimation of optimum TMD parameters for a preselected damping ratio of the main structure. Considering different mass ratios and structural periods, they utilized numerous different earthquake recordings to determine critical structural responses. Then, they were evaluated with predicted parameters with an artificial neural network. Intending to propose surrogate models for a wider range of engineering applications in the areas of mechanics, structures, aerospace, etc., the innovation of this study is to introduce surrogate estimation models with considering a wider range of damping ratios for the main structure and the possible excitation loads. For this purpose, four models based on RBF, FFNN, ANFIS, and RF are proposed for the prediction of the optimal TMD parameters in damped-structure (with different critical damping ratios for the main structure) subjected to three loading cases including harmonic base acceleration, white noise acceleration, and external white noise force. Considering each loading case, a wide-range numerical optimization procedure based on the CS optimization algorithm was carried out to a data set including the optimal frequency and damping ratio of the TMD for preselected TMD mass ratios and structural damping ratios. Some statistical indices are utilized for the assessment of the validation of the proposed models. A parametric study is also done on the optimal frequency and damping ratio of the TMD for different condition loads.

The rest of this paper is organized as follows: The design problems of TMD for a damped-structure subjected to harmonic base acceleration, white noise acceleration, and external white noise force are described in Sec. 2. CS optimization algorithm is briefly introduced in Sec. 3. Section 4 presents an introduction to RBF, FFNN

ANFIS, and RF methods. The simulation results are discussed in Sec. 5. In this section, the dataset is created for the estimation of optimal TMD parameters using the CS optimization algorithm. Also, they applied to build models based on RBF, FFNN, ANFIS, and RF. A parametric study is also carried out on the optimal TMD parameters in this section. The concluding remarks are also drawn at the end section.

2. Statement of the Design Problems of TMD

TMD as a passive control device can be employed for vibration mitigation in a wide range of engineering applications such as supporting structures subjected to oscillatory forces produced by operating equipment; sensitive instruments due to vibrations of their supporting structures; tower, building and bridges subjected to wind and earthquake loads; unbalanced rotating machine in the building; wind turbines, etc. For simplicity and avoidance of complexity, the TMD is attached to an equivalent SDOF system as an equivalent model of the main system. The forces and impulses applied to the system can be considered randomly/harmonic forces or acceleration.

The design problems of TMD for three loading excitations studied in this paper are summarized in Fig. 1. The first case is an SDOF main system equipped with TMD under harmonic acceleration (HA) with frequency invariant amplitude. The second case is an SDOF main system equipped with TMD subjected to a Gaussian white-noise force (WNF) with constant power spectral density s_0. Furthermore, the third case is an SDOF main system equipped with TMD excited by a white-noise acceleration (WNA). The main parameters of the SDOF system are mass, stiffness, and viscous damping represented by m_s, k_s and c_s, respectively. Considering the main parameters of the SDOF system, the natural frequency and viscous damping ratio of the SDOF system are given by $\omega_s = \sqrt{k_s/m_s}$ and $\xi_s = c_s/2\sqrt{k_s m_s}$, respectively. The TMD parameters are TMD mass, TMD stiffness, and TMD viscous damping shown as m_d, k_d and c_d which a TMD frequency and viscous damping ratio as $\omega_d = \sqrt{k_d/m_d}$ and $\xi_d = c_d/2\sqrt{k_d m_d}$, respectively. The design problem of TMD is to find the optimal tuning frequency ratio $f_d^{\text{opt}} = \omega_d/\omega_s$ and optimal TMD damping ratio ξ_d^{opt} for a preselected TMD mass ratio $\mu = m_d/m_s$. Considering $x_s(t)$ and $x_T(t)$ as the displacement of the main system and the TMD relative to the base, the cost function of the TMD optimal design problem for the first case can be defined as the ratio of the vibration amplitude of the main mass to the input amplitude represented by $R_{\text{HA}} = \frac{\omega_s^2|x_s|}{G}$ in which G is the acceleration amplitude which is independent of frequency. Also, γ is the ratio of load frequency to the natural frequency of the SDOF system.[4] For the second case, the cost function of the TMD optimal design problem is $R_{\text{WNF}} = \sigma^2_{xs-\text{WNF}} k_s^2/2\pi s_0 \omega_s$, where $\sigma^2_{xs-\text{WNF}}$ refers to the mean square displacement response of the main system and s_0 is the constant power spectral density of the Gaussian white-noise force.[4] By defining the response quantity of the main system as $R_{\text{WNA}} = \sigma^2_{xs-\text{WNA}} \omega_s^3/2\pi s_0$, the mean square displacement response of the main system $\sigma^2_{xs-\text{WNA}}$ is considered as the cost function of the TMD optimal design problem for the third case.[24]

Case study	Description of the model and optimization problem

a) HA

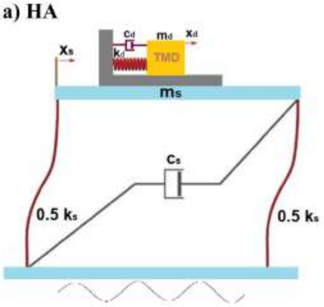

Equation of motion:

$$\begin{bmatrix} m_s & 0\\ 0 & m_d\end{bmatrix}\begin{Bmatrix}\ddot{x}_s(t)\\ \ddot{x}_d(t)\end{Bmatrix} + \begin{bmatrix} c_s+c_d & -c_d\\ -c_d & c_d\end{bmatrix}\begin{Bmatrix}\dot{x}_s(t)\\ \dot{x}_d(t)\end{Bmatrix} + \begin{bmatrix} k_s+k_d & -k_d\\ -k_d & k_d\end{bmatrix}\begin{Bmatrix}x_s(t)\\ x_d(t)\end{Bmatrix} = \begin{Bmatrix}m_s\\ m_d\end{Bmatrix} G e^{iwt}$$

Optimization problem:

$$\begin{cases}\text{Find } f_d^{opt} \text{ and } \xi_d^{opt}\\ \text{minimize } \left[\text{maximum } R_{HA}(\mu,\gamma,\xi_s,f_d,\xi_d)=\sqrt{\dfrac{C}{D}}\right]\\ \text{Subjected to } f_d>0, 0\le\xi_d\le 1\end{cases}$$

$$C = [f^2(1+\mu)-\gamma^2]^2 + 4\gamma^2 f^2 \xi_d^2(1+\mu)^2$$

$$D = [\mu f^2\gamma^2 - (\gamma^2-1)(\gamma^2-f^2) + 4 f\xi_d\xi_s\gamma^2]^2 + 4\gamma^2[f\xi_d(\gamma^2+\mu\gamma^2-1)+\xi_s(\gamma^2-f^2)]^2$$

b) WNF

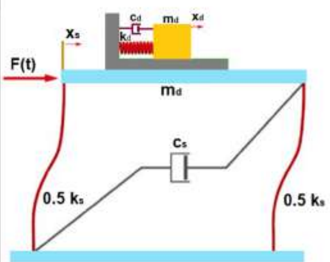

Equation of motion:

$$\begin{bmatrix} m_s & 0\\ 0 & m_d\end{bmatrix}\begin{Bmatrix}\ddot{x}_s(t)\\ \ddot{x}_d(t)\end{Bmatrix} + \begin{bmatrix} c_s+c_d & -c_d\\ -c_d & c_d\end{bmatrix}\begin{Bmatrix}\dot{x}_s(t)\\ \dot{x}_d(t)\end{Bmatrix} + \begin{bmatrix} k_s+k_d & -k_d\\ -k_d & k_d\end{bmatrix}\begin{Bmatrix}x_s(t)\\ x_d(t)\end{Bmatrix} = \begin{Bmatrix}F(t)\\ 0\end{Bmatrix}$$

Optimization problem:

$$\begin{cases}\text{Find } f_d^{opt} \text{ and } \xi_d^{opt}\\ \text{minimize } R_{WNF}(\mu,\xi_s,f_d,\xi_d)=\dfrac{A}{B}\\ \text{Subjected to } f_d>0, 0\le\xi_d\le 1\end{cases}$$

$$A = \xi_d[1-f^2(2+\mu)+f^4(1+\mu)^2] + \mu f^3\xi_s + 4f^2\xi_d^3(1+\mu) + 4f\xi_d^2\xi_s[1+f^2(1+\mu)] + 4f^2\xi_d\xi_s^2$$

$$B = 4[\mu f\xi_s^2 + \xi_T\xi_s\{1-2f^2+f^4(1+\mu)^2+4f^2\xi_T^2(1+\mu) + 4f\xi_T\xi_s[1+f^2(1+\mu)]+4f^2\xi_s^2\}+\mu f^3\xi_s^2]$$

c) WNA

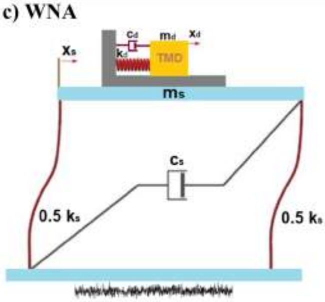

Equation of motion:

$$\begin{bmatrix} m_s & 0\\ 0 & m_d\end{bmatrix}\begin{Bmatrix}\ddot{x}_s(t)\\ \ddot{x}_d(t)\end{Bmatrix} + \begin{bmatrix} c_s+c_d & -c_d\\ -c_d & c_d\end{bmatrix}\begin{Bmatrix}\dot{x}_s(t)\\ \dot{x}_d(t)\end{Bmatrix} + \begin{bmatrix} k_s+k_d & -k_d\\ -k_d & k_d\end{bmatrix}\begin{Bmatrix}x_s(t)\\ x_d(t)\end{Bmatrix} = \begin{Bmatrix}m_s\\ m_d\end{Bmatrix}\ddot{x}_g(t)$$

Optimization problem:

$$\begin{cases}\text{Find } f_d^{opt} \text{ and } \xi_d^{opt}\\ \text{minimize } R_{WNA}(\mu,\xi_s,f_d,\xi_d)=\dfrac{E}{B}\\ \text{Subjected to } f_d>0, 0\le\xi_d\le 1\end{cases}$$

$$B = 4[\mu f\xi_s^2 + \xi_d\xi_s\{1-2f^2+f^4(1+\mu)^2+4f^2\xi_d^2(1+\mu) + 4f\xi_d\xi_s[1+f^2(1+\mu)]+4f^2\xi_s^2\}+\mu f^3\xi_s^2]$$

$$E = \xi_d[1-f^2(2-\mu)(1+\mu)+f^4(1+\mu)^4] + \xi_s[\mu^2 f+\mu f^3(1+\mu)^2] + 4f^2\xi_d^3(1+\mu)^3 + 4f\xi_d^2\xi_s(1+\mu)^2[1+f^2(1+\mu)] + 4f^2\xi_d\xi_s^2(1+\mu)^2$$

Fig. 1. The design problems of TMD for three loading excitations.

3. Cuckoo Search Optimization Algorithm

The CS optimization algorithm was first proposed by Yang and Deb.[40] To explore search space better than the standard Gaussian process, the Lévy flights are used in this algorithm. Also, the switching probability restores a balance between local search and global search exploration. The population size, n, and switching probability, p_a, are the effective parameter on the performance of the algorithm, whereas the other two parameters of the CS, i.e. the step-size, α, and Lévy flights exponent, β, are often considered constants as 0.1 and 1.5, respectively, without noticeable effect on its performance.[41–43] Using Lévy flight, the new solution, x_i^{t+1}, for the ith cuckoo is obtained as[41]

$$x_i^{t+1} = x_i^t + \alpha \oplus \text{Lévy}(\beta), \tag{1}$$

where $\oplus$ represents the entry-wise multiplications. Also, $\alpha > 0$ and β are the step-size and the Lévy flights exponent and obtained by the following equations:

$$\alpha = \alpha_0 \oplus (x_j^t - x_i^t), \tag{2}$$

$$\text{Lévy}(\beta) = \frac{u}{|v|^{\frac{1}{\beta}}}, \tag{3}$$

where u and v are the two parameters with zero means and variances represented in Eq. (4).

$$\sigma_u = \left\{\frac{G(1+\beta)\sin(\pi\beta/2)}{G[(1+\beta)/2]\beta 2^{(\beta-1)}/2}\right\}^{1/\beta}, \quad \sigma_v = 1. \tag{4}$$

To escape from the local optima, the CS generates a new solution, x_i^{t+1}, using the following equation[44]:

$$x_i^{t+1} = x_i^t + r \oplus H(p_a - \epsilon) \oplus (x_j^t - x_k^t), \tag{5}$$

where $H(\cdot)$ represents the Heaviside function. It is a non-continuous function whose value is zero for a negative input and one for positive input. Furthermore, x_j^t and x_k^t refer to two different solutions; r and ϵ are some random numbers with uniform distribution in [0,1]. The successful applications of the CS optimization algorithm in the optimization structural problems have been reported in Refs. 45–48.

4. An Introduction on RBF, FFNN, ANFIS, and RF Techniques

AI techniques have been successfully applied for sciences and engineering applications. A brief review of some AI techniques including RBF, FFNN ANFIS, and RF techniques are introduced in this section as follows:

4.1. *Radial basis function neural network*

RBF neural network is a well-performing, prospective model for solving supervised learning problems. As can be seen from Fig. 2, this network can be depicted as a multi-input single-output (MISO) system with the input, hidden, and output layers. The hidden layer is formed based on nonlinear RBF activation functions, the number, and parameters that are determined in training the network. The output layer offers a linear combination of output weights. In case of a feature space of N training samples with inputs of $X = (X_1, X_2, \ldots, X_N)$, and expected output of

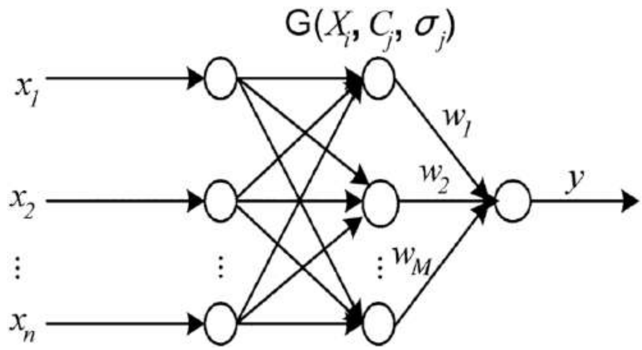

Fig. 2. The RBF neural network structure.[49]

$Y = (y_1, y_2, \ldots, y_N)$, the output of the jth node in the hidden layer is obtained based on input X_i as follows:

$$G(X_i, C_j, \sigma_j) = \exp\left(-\frac{\|X_i - C_j\|}{2\sigma^2}\right) = \exp(-\gamma\|X_i - C_j\|). \tag{6}$$

Here, $X_i = (x_{i1}, x_{i2}, \ldots, x_{in})^T, 1 \leq i \leq N$ is the ith input vector, $C_j = (c_{j1}, c_{j2}, \ldots, c_{jn})^T$ and σ_j are the center and width of the Gaussian function of the j–h node in the hidden layer. The parameter γ is also known as the RBF network parameter[49] and calculated as

$$\gamma = \frac{1}{2\sigma^2}. \tag{7}$$

The expected network output for ith input X_i is as follows:

$$y_i = \sum_{j=1}^{M} G(X_i, C_j, \sigma_j) w_j + e_i. \tag{8}$$

In Eq. (7), w_j is the weight connecting the jth neurons in the hidden layer to the output neurons, M indicates the hidden layer's number of neurons, y_i denotes the ith expected output and e_i is the error of fitting.[49] With a simple shift in Eq. (8) e_i can be obtained as

$$e_i = y_i - \sum_{j=1}^{M} G(X_i, C_j, \sigma_j) w_j. \tag{9}$$

Here, the orthogonal least squares algorithm is used to select the central Gaussian parameter. This method is used to minimize the total error of the functions toward training the output weight as follows[49]:

$$\min E = \frac{1}{2}\sum_{i=1}^{N} e_i^2. \tag{10}$$

4.2. *Feed-forward neural network*

Artificial neural networks the are mathematical models that mimic biological brain neural networks. In recent decades, due to their development speed as well as their applications in various fields, artificial neural networks have been considered by many scientific communities and are still expanding. Figure 3 shows an example of an FFNN.

The FFNNs are suitable for solving some of the most complex and varied problems. The training of these networks is mainly done with a supervised algorithm known as the backpropagation (PB) algorithm.[51] The BP algorithm is designed to minimize the training mean square error, in a set of iterations based on the gradient of the weight vector's loss function, to find the optimal values of the weight vector. Although the popularity and wide-spread use of neural networks, the use of these networks pose challenges such as determining the appropriate neural network's size and optimal structure, the complexity of understanding the relationship between weight change and input and output behavior during training. Besides, manipulating learning parameters is very difficult and sometimes not possible. In terms of hardware implementation, they are also costly.

4.3. *Adaptive neuro-fuzzy inference system (ANFIS)*

An adaptive neuro-fuzzy inference system is an integration of fuzzy systems and neural networks. A fuzzy inference system (FIS) is applied to the inputs and its membership function parameters which are tuned in progress based on the backpropagation algorithm only or in combination with the least-squares type

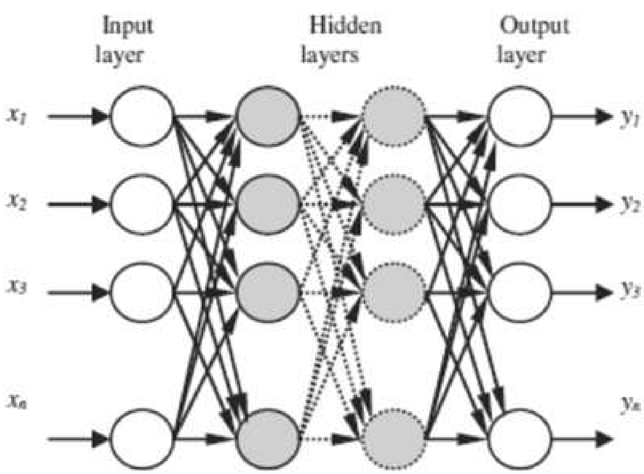

Fig. 3. The structure of an FFNN.[50]

approach.[52] One of the most common fuzzy inference systems is the Takagi–Sugeno–Kang (TSK) fuzzy model. TSK fuzzy model is simple as few rules are required and estimation of parameters can be performed based on numerical data obtained by optimization methods.[53]

The structure of an adaptive neuro-fuzzy inference system consists of the following five layers:

- *Layer I, fuzzification*: In this layer, the membership functions of the input parameters are determined.
- *Layer II, rule*: The exciting strengths of the rules are generated.
- *Layer III*: Normalization of the firing rules is performed.
- *Layer IV*: In this layer, the contribution of each rule is obtained by applying the firing strength to the consequent membership function.
- *Layer V, Defuzzification*: The overall output of the system is obtained.

Figures 4(a) and 4(b) depict the fuzzy reasoning and the corresponding structure of a TSK model with one output (f) and two inputs (x, y), and the governing rules

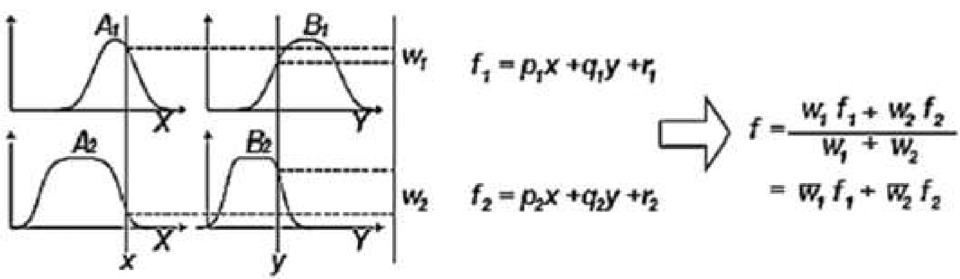

(a)

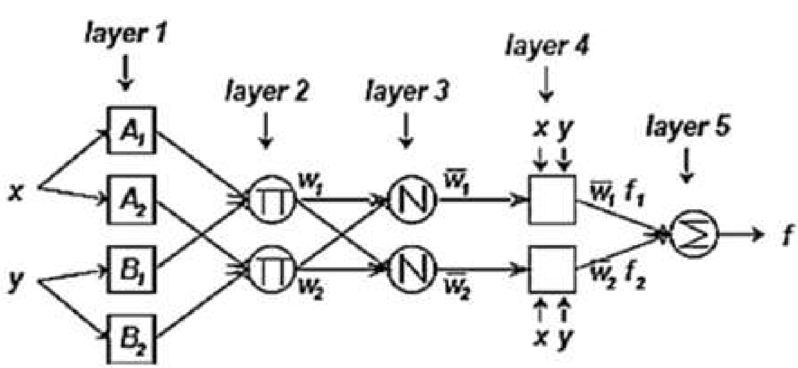

(b)

Fig. 4. (a) First-order Sugeno fuzzy model; (b) Architecture of equivalent ANFIS.[54]

expressed as follows:

Rule 1: if $x = A_1$ and $y = B_1$, then $f_1 = p_1x + q_1y + r_1$.
Rule 2: if $x = A_2$ and $y = B_2$, then $f_2 = p_2x + q_{12}y + r_2$.

One of the strengths and advantages of ANFIS is that a learning process is performed in hybrid mode to properly estimate the premise and consequent parameters.[54] In this method, the learning process is performed in two independent stages. The first stage is an adaptation of the learning weight and the second stage is an adaptation to nonlinear membership functions. This method can be a useful algorithm by reduction of complexity as well as the enhancement of learning efficiency.[55] More detail of the ANFIS is found in Ref. 56.

4.4. *Random forest model*

Random forest is a supervised learning algorithm that is used in classification and regression. This method was first introduced by Berman.[57] It is an ensemble method consisted of a simple combination of predictors and its performance. It has been improved due to the use of predictions obtained by the set of models that make up the ensemble.[58] One of the most important challenges in using decision trees is to prevent overfitting and increase accuracy, which can be achieved by producing many decision trees and collecting their results to achieve this goal.[59] RF regressor works by dividing the training dataset equally and randomly into a certain number of groups. Each dataset is then given as input to a decision tree, which then processes the dataset and gives its own output. The RF Regressor takes into account the prediction from all the trees and then arrives to a result, generally obtained by averaging out the predictions from all the decision trees.[60] The construction of a random forest is presented step by step as follows[61]:

(1) For $k \leftarrow 1$ to M do
(2) $D_k \leftarrow$ Bootstrap(D)
(3) $h_k \leftarrow$ Random Feature Selection in Decision Tree (D_k, F)
(4) End of for
(5) return $\cup h_k$

In the above pseudocode, D represents the training set, M denotes the number of models in the group, and F represents the number of attributes used by each node.

5. Results and Discussion

This section is divided into three subsections. First, a dataset of optimal TMD parameters for the damped-structure subjected to different excitations including WNF, HA, and WNA are collected using an optimization procedure based on the CS optimization algorithm. In the second subsection, the RBF, FFNN, ANFIS, and RF models are proposed for the prediction of optimal TMD parameters. Considering four statistical indices, the accuracy and validation of the models for estimation of optimal TMD parameters are evaluated and compared. A parametric study is carried out to assessments the effects of TMD mass ratio and structural damping ratio on the optimum TMD frequency and damping ratio for different loading excitations.

5.1. *Data set using CS optimization algorithm*

The CS optimization algorithm is utilized for the optimal design problem of TMD in the main system subjected to three types of excitations: WNF, HA and WNA. The population size, switching probability, step-size parameter, and the Lévy flight exponent of the CS are adopted as $n = 20$, $p_a = 0.25$, $\alpha = 0.1$, and $\beta = 1.5$, respectively. For a preselect mass ratio as $\mu = [0.01, 0.002, 0.004, 0.006, 0.008, 0.010, 0.015, 0.020, 0.025, 0.030, 0.035, 0.040, 0.045, 0.050, 0.055, 0.060, 0.065, 0.070, 0.075, 0 .080, 0.085, 0.090, 0.095, 0.100]$ and different damping ratio of the main structure as $\xi_s = [0, 0.01, 0.02, 0.03, 0.05, 0.075, 0.1]$, the optimal tuning frequency and damping ratio of the TMD system are designed for three loading cases. Hence, a total of 161 optimization problems is performed for each loading case. The results are illustrated in Fig. 5.

5.2. *RBF, FFNN, ANFIS, and RF models for prediction of optimal TMD parameters*

In this study, a training set of 70% of the dataset and a test set of 30% of the dataset are selected for training and test of the proposed models. Furthermore, the spider machine learning toolbox is utilized to train an RBF neural network with three centers. The RBF network parameter i.e. Ɣ is obtained to attain the best training results. The values of Ɣ for the estimation of optimal frequency ratio of TMD are selected as 7, 1, and 40 for the damped structure under WNF, HA, and WNA excitations, respectively. Similarly, the corresponding values of Ɣ for the estimation of the optimal frequency ratio of TMD are considered as 90, 400, and 90, respectively. The feed-forward neural network is also trained based on the scaled conjugate gradient backpropagation method. The models based on ANFIS are also implemented based on a Sugeno-type fuzzy inference system using Fuzzy c-means (FCM) clustering with 5 clusters and neural network optimized by a hybrid combination of least squares estimation and the backpropagation method.

A random forest model is created in Google Colab that provides the ability to write and run Python in the browser, with zero configuration, free access to GPUs, and easy sharing. The implementation of random forest regression is discussed in detail in Ref. 62. The setting of Hyperparameter is more related to experimental results than to theory, and our method for determining the optimal settings of these hyperparameters is to examine different combinations of values for effective parameters. Model evaluation based solely on training data sets without considering other data may lead to a phenomenon called "overfitting", which often reflects the

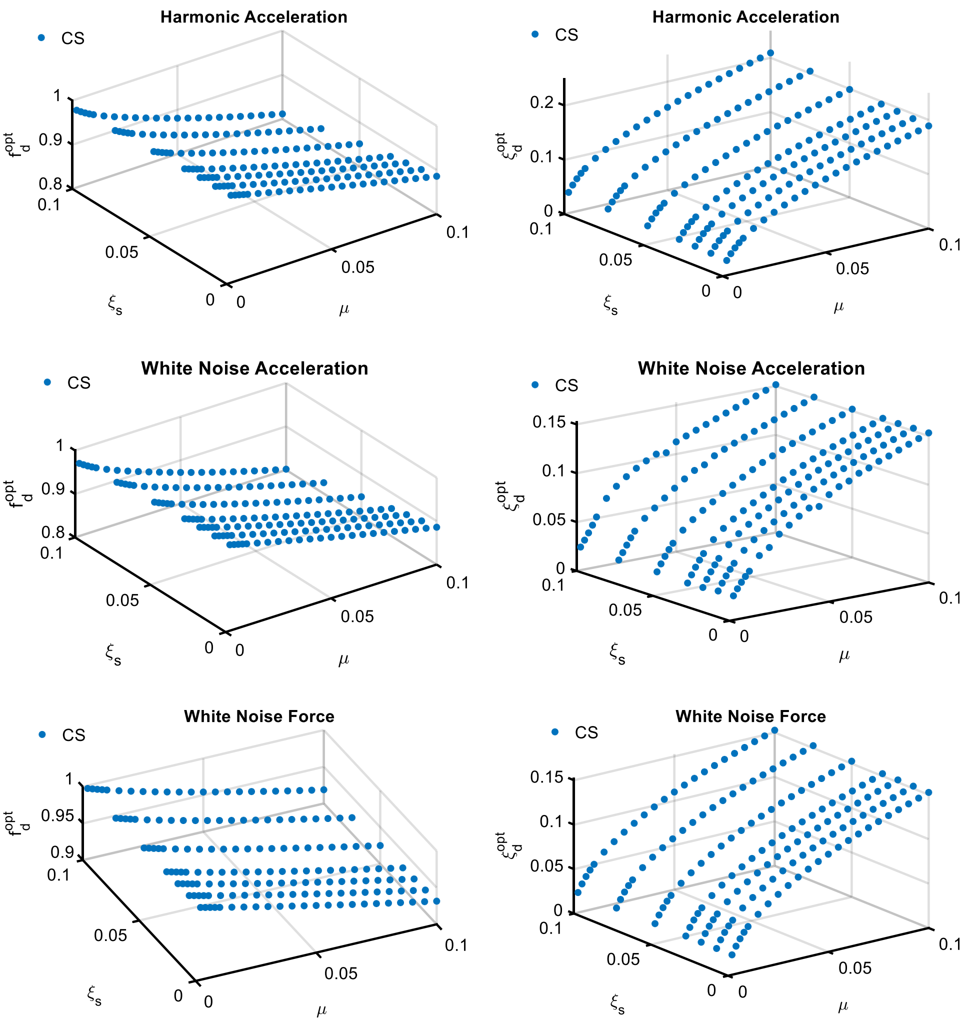

Fig. 5. Optimal tuning frequency and damping ratio of the TMD system for three loading cases.

excellent performance in the train set and the poor performance in the test set. According to the data in each data set, setting some hyperparameters can affect the final results, and in fact, setting other parameters is ineffective. Therefore, the default value is considered for them. The default values for various hyperparameters such as "min_samples_leaf", "min_sample_split", "max_leaf_nodes", "max_depth", "max_features", "max_sample", are considered in this study, but, the parameters affected on the model performance considering "overfitting" are investigated. For this purpose, by setting different values in the valid domain, for each of the parameters as well as combining them and observing the changes in the training and test data set, the optimal value of that hyperparameter is selected. For example in the

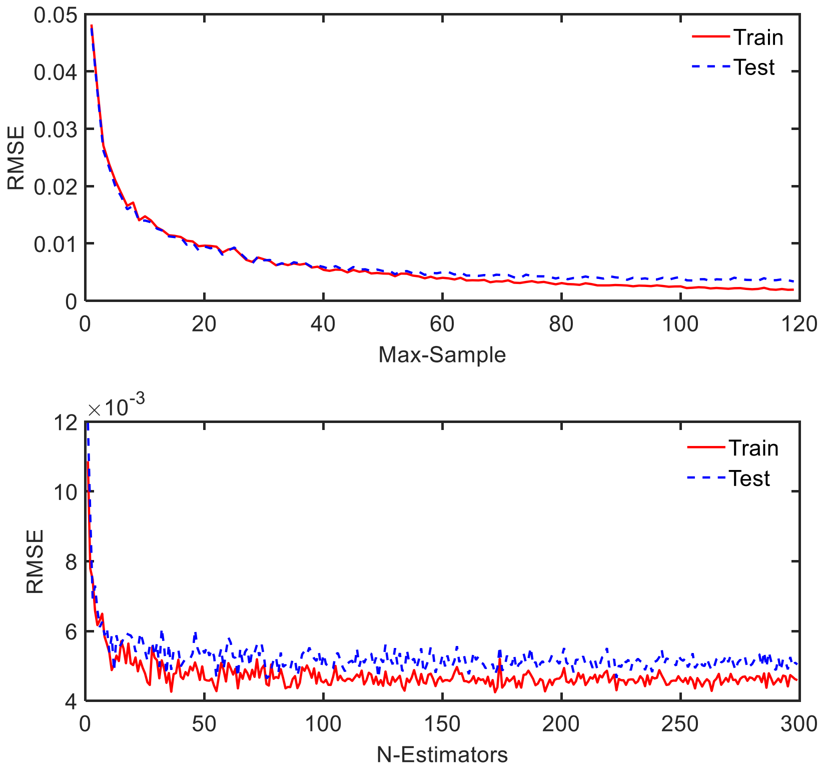

Fig. 6. An example of how setting "Max_sample" and "N_estimators" by viewing RMSE in the RF model.

estimation model for frequency ratio of TMD in WNF loading case, the best values for "Max_sample" and "N_estimators" are found as 60 and 150, as shown in Fig. 6, because after the values, no significant decrease is observed in RMSE values, while selecting their higher values increases the complexity of the model. Table 1 shows listed the random forest hyperparameter tuned for each of the datasets.

Four statistical indices, including root-mean-square error (RMSE), coefficient of determination (R^2), confidence index (CI) and mean absolute error (MAE) are considered to evaluate the accuracy and validation of the proposed models for the estimation of optimal TMD parameters in three loading cases. The mentioned statistical indices can be defined as:

$$\mathrm{RMSE} = \sqrt{\frac{\sum_{i=1}^{N}(y_o - y_p)^2}{N}}, \tag{11}$$

$$R^2 = 1 - \frac{\sum_{i=1}^{N}(y_o - y_p)^2}{\sum_{i=1}^{N}(y_o - \bar{y})^2}, \tag{12}$$

$$\mathrm{MAE} = \frac{\sum_{i=1}^{N}|y_o - y_p|}{N}, \tag{13}$$

Table 1. Random forest hyperparameter tuned for each of the datasets.

Optimal TMD parameter	Excitation	N_estimators	Max_samples
f^{opt}	WNF	150	60
	HA	170	40
	WNA	80	50
ξ_d^{opt}	WNF	110	121
	HA	100	60
	WNA	150	40

Table 2. Statistical indices for the damped-structure under HA excitation.

Model	Optimal TMD parameter	Data	RMSE	R^2	CI	MAE
RBF	ξ_d^{opt}	Test	0.005118	0.989469	0.986997	0.004195
		Train	0.005768	0.987157	0.983773	0.004599
		Total	0.005614	0.987716	0.984566	0.004499
	f^{opt}	Test	0.002714	0.996469	0.995647	0.002260
		Train	0.003260	0.995056	0.993796	0.002464
		Total	0.003133	0.995399	0.994252	0.002413
FFNN	ξ_d^{opt}	Test	0.000418	0.999930	0.999913	0.000308
		Train	0.000402	0.999938	0.999922	0.000298
		Total	0.000406	0.999936	0.999920	0.000301
	f^{opt}	Test	0.000160	0.999988	0.999985	0.000132
		Train	0.000129	**0.999992**	**0.999990**	**0.000101**
		Total	0.000137	**0.999991**	**0.999989**	**0.000109**
ANFIS	ξ_d^{opt}	Test	**0.000353**	**0.999950**	**0.999949**	**0.000257**
		Train	**0.000395**	**0.999940**	**0.999938**	**0.000292**
		Total	**0.000385**	**0.999942**	**0.999941**	**0.000284**
	f^{opt}	Test	**0.000138**	**0.999991**	**0.999989**	**0.000108**
		Train	**0.000150**	0.999990	0.999988	0.000117
		Total	**0.000147**	0.999990	0.999988	0.000115
RF	ξ_d^{opt}	Test	0.002737	0.996989	0.999913	0.002035
		Train	0.002286	0.997985	0.999940	0.001781
		Total	0.002406	0.997744	0.999934	0.001845
	f^{opt}	Test	0.005650	0.984696	0.999584	0.004052
		Train	0.005606	0.985374	0.999596	0.004061
		Total	0.005617	0.985210	0.999593	0.004059

Table 3. Statistical indices for the damped-structure under WNF excitation.

Model	Optimal TMD parameter	Data	RMSE	R^2	CI	MAE
RBF	ξ_d^{opt}	Test	0.004172	0.988729	0.986054	0.003623
		Train	0.004592	0.986884	0.983427	0.003434
		Total	0.004491	0.987331	0.984072	0.003576
	f^{opt}	Test	0.001098	0.997692	0.997135	0.000902
		Train	0.001239	0.997113	0.996378	0.000967
		Total	0.001205	0.997255	0.996566	0.000951
FFNN	ξ_d^{opt}	Test	0.000127	0.999990	0.999987	0.000093
		Train	0.000111	0.999992	0.999990	0.000081

Table 3. (*Continued*)

Model	Optimal TMD parameter	Data	RMSE	R^2	CI	MAE
		Total	0.000115	0.999992	0.999990	0.000084
	f^{opt}	Test	0.000096	0.999982	0.999978	**0.000072**
		Train	**0.000088**	0.999985	0.999982	0.000062
		Total	0.000090	0.999985	0.999981	0.000070
ANFIS	ξ_d^{opt}	Test	0.000185	0.999979	0.999973	0.000146
		Train	0.000171	0.999982	0.999981	0.000139
		Total	0.000175	0.999981	0.999980	0.000140
	f^{opt}	Test	**0.000077**	**0.999985**	**0.999985**	0.000074
		Train	0.000089	**0.999989**	**0.999989**	**0.000062**
		Total	**0.000080**	**0.999988**	**0.999988**	**0.000065**
RF	ξ_d^{opt}	Test	**0.000101**	**0.999993**	**1.000000**	**0.000086**
		Train	**0.000082**	**0.999996**	**1.000000**	**0.000065**
		Total	**0.000087**	**0.999995**	**1.000000**	**0.000070**
	f^{opt}	Test	0.001486	0.995771	0.999945	0.001054
		Train	0.001325	0.996698	0.999956	0.000995
		Total	0.001366	0.996471	0.999953	0.001010

$$\text{CI} = \text{EF} \times D, \tag{14}$$

where y_o refers to the observed data given by the optimization procedure based on CS optimization algorithm and y_p is the data predicted by the proposed models,

Table 4. Statistical indices for the damped-structure under WNA excitation.

Model	Optimal TMD parameter	Data	RMSE	R^2	CI	MAE
RBF	ξ_d^{opt}	Test	0.003954	0.989790	0.987465	0.003382
		Train	0.004517	0.987281	0.996763	0.003636
		Total	0.004384	0.987885	0.984810	0.003573
	f^{opt}	Test	0.004569	0.990696	0.988411	0.003718
		Train	0.005074	0.988851	0.985905	0.003959
		Total	0.004954	0.989300	0.986521	0.003899
FFNN	ξ_d^{opt}	Test	**0.001690**	**0.998136**	0.997679	0.001105
		Train	**0.001239**	**0.999043**	0.998801	0.000915
		Total	**0.001365**	**0.998826**	0.998531	**0.000962**
	f^{opt}	Test	0.000239	0.999974	0.999968	**0.000081**
		Train	0.000701	0.999787	0.999732	**0.000032**
		Total	0.000619	0.999833	0.999790	**0.000026**
ANFIS	ξ_d^{opt}	Test	0.001986	0.997424	0.997366	**0.000884**
		Train	0.002129	0.997173	0.997108	**0.001144**
		Total	0.002095	0.997234	0.997170	0.001079
	f^{opt}	Test	**0.000109**	**0.999995**	**0.999995**	0.000088
		Train	**0.000114**	**0.999994**	**0.999993**	0.000085
		Total	**0.000113**	**0.999995**	**0.999994**	0.000086
RF	ξ_d^{opt}	Test	0.002298	0.996552	**0.999922**	0.001586
		Train	0.002119	0.997202	**0.999935**	0.001492
		Total	0.002165	0.997046	**0.999932**	0.001516
	f^{opt}	Test	0.004813	0.989675	0.999708	0.003516
		Train	0.004066	0.992843	0.999794	0.002828
		Total	0.004264	0.992073	0.999772	0.002999

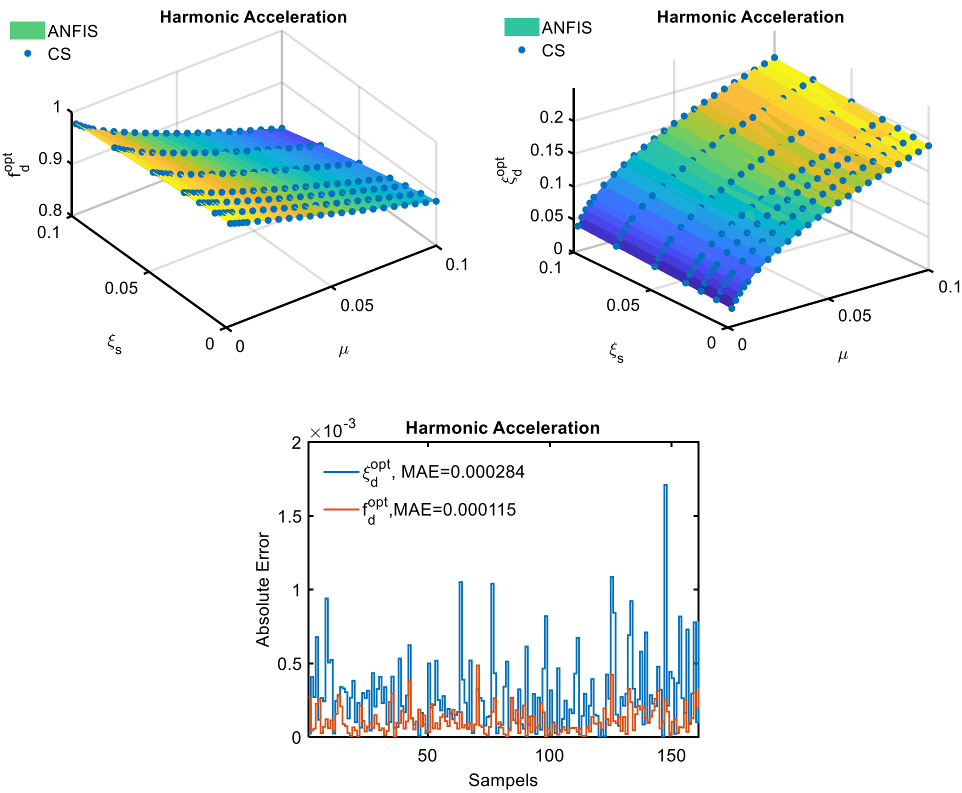

Fig. 7. A comparison between the TMD design parameters estimated by ANFIS models and optimized by CS optimization algorithm in damped structures subjected to HA.

respectively. N is the number of samples and $\bar{y}$ is the mean value of the desired data. Moreover, D and EF are the agreement index and the model efficiency factor defined as follows:

$$D = 1 - \frac{\sum_{i=1}^{N}(y_o - y_p)^2}{\sum_{i=1}^{N}(|y_p - \bar{y}_o| + |y_o - \bar{y}_o|)} \quad 0 \ll D \ll 1, \tag{15}$$

$$\mathrm{EF} = 1 - \frac{\sum_{i=1}^{N}(y_o - y_p)^2}{\sum_{i=1}^{N}(y_o - \bar{y}_o)^2} \quad 0 \ll EF \ll 1, \tag{16}$$

where $\bar{y}_o$ is the mean value of the observed data. The statistical indices for the training set, test set, and total set data of the RBF, FFNN, ANFIS, and RF models are reported in Tables 2–4 for the damped structure under WNF, HA, and WNA excitations, respectively.

Lower values for MAE and RMSE of the models indicate a better fitness while approaching the statistical indices values of R^2 and CI to one represents better fitness between the observed and predicted data. Considering the results given for

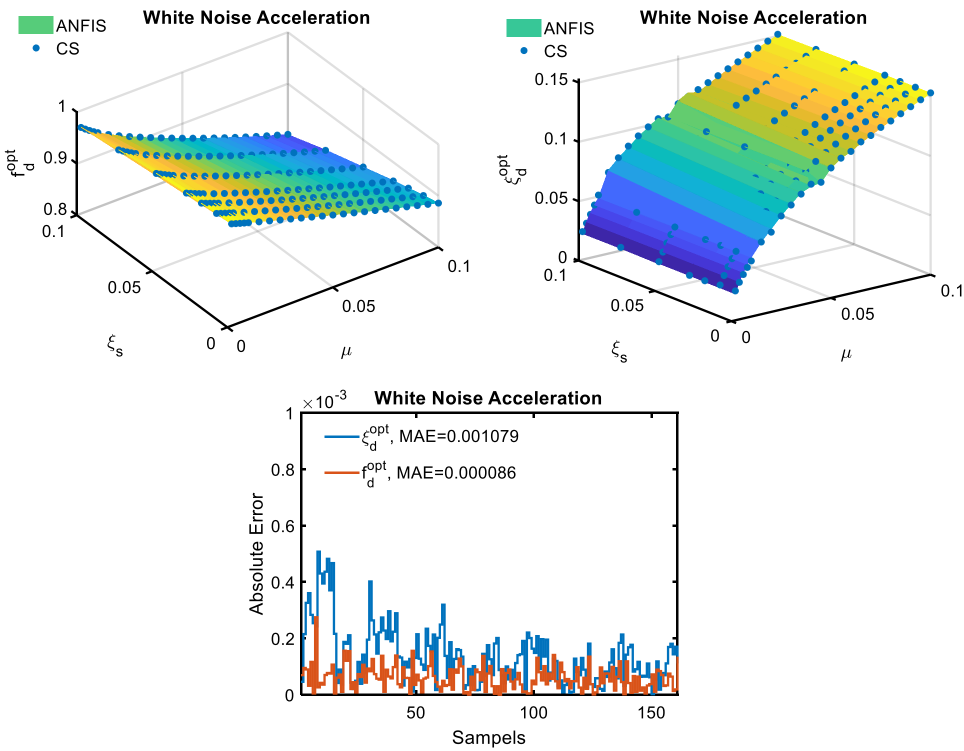

Fig. 8. A comparison between the TMD design parameters estimated by ANFIS models and optimized by CS optimization algorithm in damped structures subjected to WNA.

the total set data of each model, the best result for the prediction of optimal TMD frequency and damping ratio are bolded in these tables. As can be seen, the RBF, FFNN, ANFIS, and RF models can exhibit a high degree of fitness. Hence, the accuracy and capability of the proposed models for the prediction of optimum TMD parameters are confirmed. The proposed models eliminate the need for designers for time-consuming numerical analyses in the conventional optimization methods to determine the optimal TMD parameters which is a boring task.

The overall results show that the best and the worst performance of the models for estimation of the optimal TMD frequency and damping ratio are given for ANFIS and RBF models, respectively. The surface outcome from the ANFIS model for the prediction of optimal TMD frequency and damping ratio for different TMD mass ratios and structural damping ratios are compared with those given by the optimization procedure based on the CS algorithm in Figs. 7–9. The corresponding scatters plots of the observed versus predicted set using the ANFIS models are also illustrated in the figures. A good match of the results obtained from the optimal estimation of TMD parameters using the ANFIS model and the results given by the CS algorithm is observed. It is demonstrated that the ANFIS models can estimate the optimal TMD parameters with appropriate accuracy. The absolute error and mean absolute

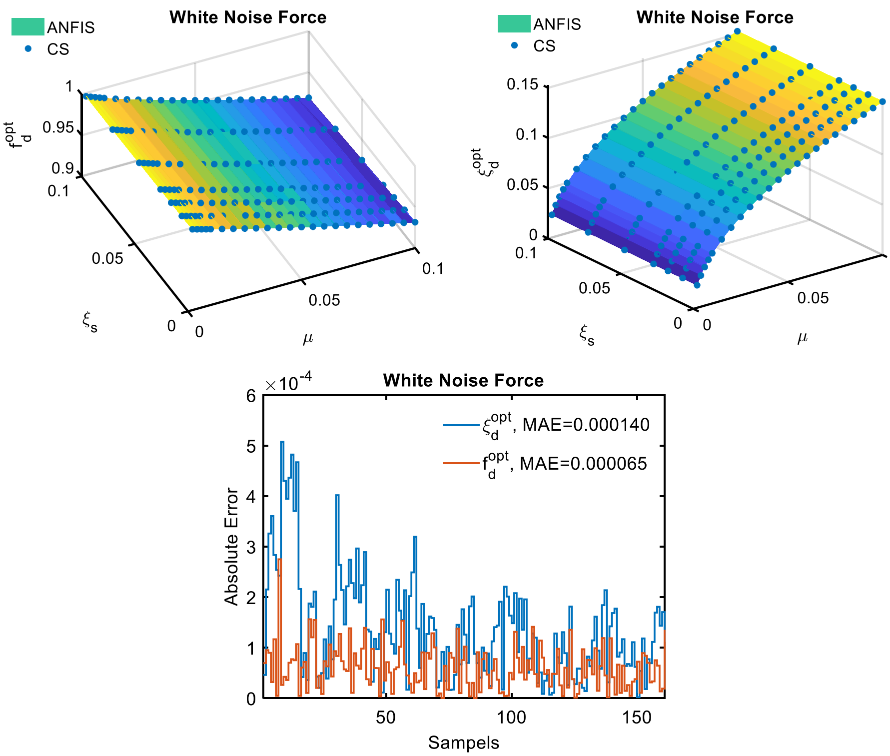

Fig. 9. A comparison between the TMD design parameters estimated by ANFIS models and optimized by CS optimization algorithm in damped structures subjected to WNF.

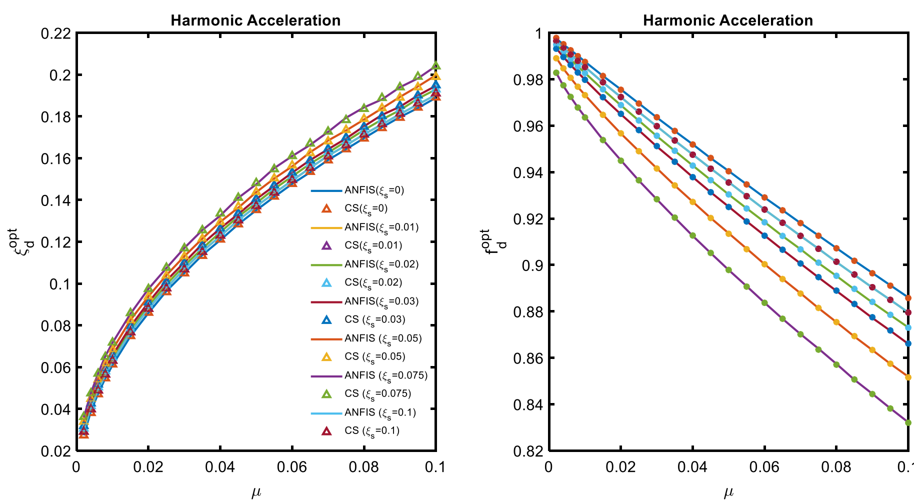

Fig. 10. The effects of TMD mass ratio and structural damping ratio on the optimum TMD frequency and damping ratio in the damped structure subjected to HA.

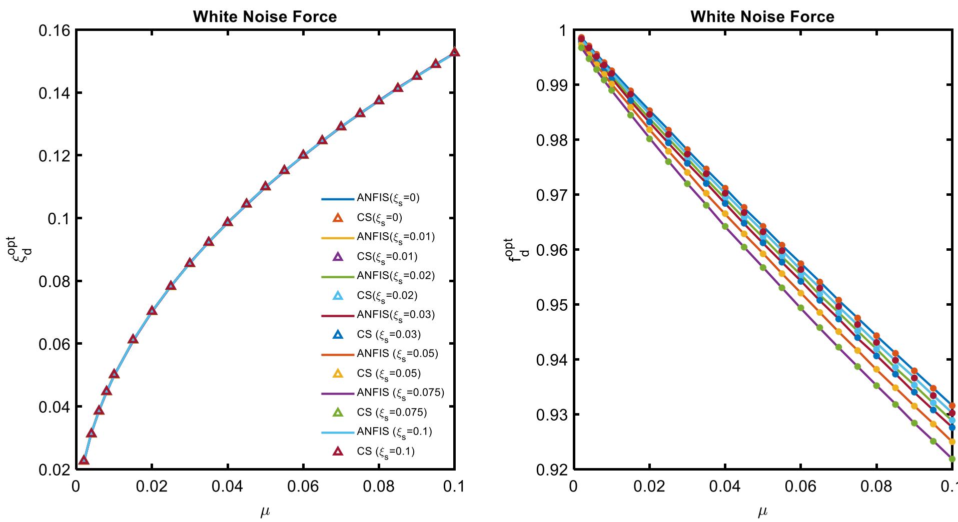

Fig. 11. The effects of TMD mass ratio and structural damping ratio on the optimum TMD frequency and damping ratio in a damped structure subjected to WNF.

error between the observed data using CS and the corresponding data predicted by ANFIS are also shown in the figures.

5.3. *Parametric studies*

At the end of this section, the effects of the TMD mass ratio and structural damping ratio on the optimum TMD frequency and damping ratio for different loading excitations are investigated in Figs. 10–12. For comparison purposes, the curve predicted by the ANFIS method is also drawn. As can be seen, the ANFIS model as a surrogate model can accurately predict the optimal TMD parameters. The results of the damped structure under HA excitation indicate the optimum TMD frequency ratio is decreased and the optimal TMD damping ratio is increased by increasing the TMD mass ratio. For a TMD mass ratio, the optimal TMD frequency is decreased with increasing structural damping ratio and the optimal TMD damping ratios are increased.

Considering the results shown in Fig. 11 for the WNF loading case, it is concluded that by increasing TMD mass ratio, the optimal TMD frequency ratio decreases, and the optimal TMD damping ratio is increased, however, these changes are with a smoother trend than the HA loading case. As can be seen, the optimal TMD damping ratio, in this case, is independent of the structural damping ratio. Considering the results illustrated in Fig. 12, it is found similar results for the WNA loading case with those given for the optimal TMD frequency in the WNF loading case. Nevertheless, for a certain amount of the TMD mass ratio, its optimal values vary over a wider range. For example, the optimal TMD frequency ratios for TMD mass ratio $\mu = 0.1$ are changed in a range between 0.8 to 0.9 depending on the values of the structural

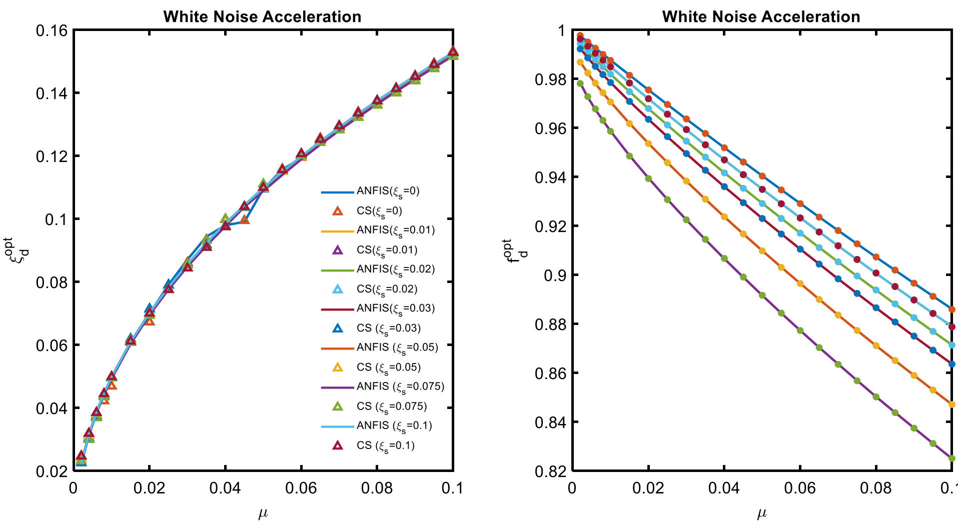

Fig. 12. The effects of TMD mass ratio and structural damping ratio on the optimum TMD frequency and damping ratio in the damped structure subjected to WNA.

damping ratio. The optimal TMD damping ratio is also independent of the structural damping ratio.

6. Conclusion

This study aimed to propose new models based on AI techniques to predict the optimal TMD parameters. For this purpose, an SDOF damped structure equipped with TMD subjected to three loading excitations including WNF, HA, and WNA were considered. The optimization design problems of the TMD parameters for the three cases were introduced. Dataset including optimal frequency and damping ratio of the TMD for different TMD mass ratio and structural damping ratio for the main damped-structure in three types of excitations were created using an optimization procedure based on CS optimization algorithm. Then, four models including RBF, FFNN, ANFIS, and RF models were proposed for estimation of the optimal TMD parameters. These models eliminated the need for designers for tedious time-consuming numerical analyses to determine the optimal TMD parameters using conventional optimization methods. The concluding remarks were as follows:

(1) A high degree of fitness between the optimal TMD frequency and damping ratios observed by the CS algorithm with those predicted by the RBF, FFNN, and ANFIS models were found. Hence, the accuracy and capability of the proposed models were validated for the prediction of optimum TMD parameters.
(2) For the damped-structure subjected to HA excitation, the FFNN model gave the best results for the predation of optimal TMD frequency. Besides, the surrogate model based on ANFIS resulted in the best performance for predation of optimal

TMD damping ratio in this case. RF and FFNN models represented less error and more correlation for predation of optimal damping ratio of the TMD in the damped-structure subjected to WNF and WNA excitations, respectively.

(3) Overall, a comparison among the statistical index values investigated for the RBF, FFNN, and ANFIS models showed that the ANFIS model has less error and more correlation with the observed optimal TMD parameters using CS. Also, the worst performance for estimation of the optimal TMD parameters was archived for the RBF model, respectively.

(4) For a damped-structure subjected to HA excitation, by increasing the TMD mass ratio, the optimal frequency ratio of the TMD was decreased and the optimal damping ratio of the TMD was decreased. For a certain mass ratio, by increasing the damping ratio of the structure, the optimal TMD frequency was decreased and its optimal damping ratio was increased.

(5) Considering the results given for the damped-structure under WNF excitation, it was found that by increasing the TMD mass ratio, the optimal TMD frequency ratio was decreased and the optimal TMD damping ratio was increased. In this case, the optimal damping ratio of the TMD was independent of the structural damping ratio.

(6) Similar results were concluded for the damped-structure under WNA excitation with those given for WNF excitation. For a certain TMD mass ratio, a wide range of optimal TMD frequency was optimized for different structural damping ratios.

References

1. G. B. Warburton, Optimum absorber parameters for various combinations of response and excitation parameters, *Earthq. Eng. Struct. Dyn.* **10**(3) (1982) 381–401.
2. H. C. Tsai and G. C. Lin, Optimum tuned-mass dampers for minimizing steady-state response of support-excited and damped systems, *Earthq. Eng. Struct. Dyn.* **22**(11) (1993) 957–973.
3. T. Asami, O. Nishihara and A. M. Baz, Analytical solutions to H_∞ and H_2 optimization of dynamic vibration absorbers attached to damped linear systems, *J. Vib. Acoust.* **124**(2) (2002) 284–295.
4. S. V. Bakre and R. S. Jangid, Optimum parameters of tuned mass damper for damped main system, *Struct. Control Health Monit.* **14**(3) (2007) 448–470.
5. E. O. Ayorinde and G. B. Warburton, Minimizing structural vibrations with absorbers, *Earthq. Eng. Struct. Dyn.* **8**(3) (1980) 219–236.
6. G. B. Warburton and E. O. Ayorinde, Optimum absorber parameters for simple systems, *Earthq. Eng. Struct. Dyn.* **8**(3) (1980) 197–217.
7. G. B. Colherinhas, M. V. G. Morais, M. A. M. Shzu and S. M. Avila, Optimal pendulum tuned mass damper design applied to high towers using genetic algorithms: Two-DOF modeling, *Int. J. Struct. Stab. Dyn.* **19**(10) (2019) 1950125.
8. S. Etedali, M. Akbari and M. Seifi, MOCS-based optimum design of TMD and FTMD for tall buildings under near-field earthquakes including SSI effects, *Soil Dyn. Earthq. Eng.* **119** (2019) 36–50.

9. L. Tian, K. Rong, K. Bi and P. Zhang, A bidirectional pounding tuned mass damper and its application to transmission tower-line systems under seismic excitations, *Int. J. Struct. Stab. Dyn.* **19**(6) (2019) 1950056.
10. C. Fabrizio, A. M. de Leo and A. Di Egidio, Tuned mass damper and base isolation: A unitary approach for the seismic protection of conventional frame structures, *J. Eng. Mech.* **145**(4) (2019) 04019011.
11. Y. J. Kang, L. Y. Peng, W. Liu and Z. R. Lai, Steady-state response and damping control effect of Reid-TMD, *Int. J. Struct. Stab. Dyn.* **19**(10) (2019) 1950122.
12. A. H. Heidari, S. Etedali and M. R. Javaheri-Tafti, A hybrid LQR-PID control design for seismic control of buildings equipped with ATMD, *Front. Struct. Civil Eng.* **12**(1) (2018) 44–57.
13. M. Shahi, M. R. Sohrabi and S. Etedali, Seismic control of high-rise buildings equipped with ATMD including soil-structure interaction effects, *J. Earthq. Tsunami* **12**(3) (2018) 1850010.
14. P. Y. Lin, L. L. Chung and C. H. Loh, Semiactive control of building structures with semiactive tuned mass damper, *Comput. Aided Civil Infrast. Eng.* **20**(1) (2005) 35–51.
15. X. Guan, J. Zhang, H. Li and J. Ou, Semi-active control for benchmark building using innovative TMD with MRE isolators, *Int. J. Struct. Stab. Dyn.* **20**(6) (2020) 2040009.
16. G. L. Lin, C. C. Lin, L. Y. Lu and Y. B. Ho, Experimental verification of seismic vibration control using a semi-active friction tuned mass damper, *Earthq. Eng. Struct. Dyn.* **41**(4) (2012) 813–830.
17. M. N. Hadi and Y. Arfiadi, Optimum design of absorber for MDOF structures, *J. Struct. Eng.* **124**(11) (1998) 1272–1280.
18. M. P. Singh, S. Singh and L. M. Moreschi, Tuned mass dampers for response control of torsional buildings, *Earthq. Eng. Struct. Dyn.* **31**(4) (2002) 749–769.
19. G. B. Colherinhas, F. Petrini, M. V. G. Morais and F. Bontempi, Optimal design of passive-adaptive pendulum tuned mass damper for the global vibration control of offshore wind turbines, *Wind Energy*, in Press, (2020), doi:https://doi.org/10.1002/we.2590.
20. S. Etedali and S. Tavakoli, PD/PID controller design for seismic control of high-rise buildings using multi-objective optimization: A comparative study with LQR controller, *J. Earthq. Tsunami* **11**(3) (2017) 1750009.
21. R. B. Carneiro, Avila, S. M. and J. L. V. De Brito, Parametric study on multiple tuned mass dampers using interconnected masses, *Int. J. Struct. Stab. Dyn.* **8**(1) (2008) 187–202.
22. A. Y. Leung, H. Zhang, C. C. Cheng and Y. Y. Lee, Particle swarm optimization of TMD by non-stationary base excitation during earthquake, *Earthq. Eng. Struct. Dyn.* **37**(9) (2008) 1223–1246.
23. A. Y. T. Leung and H. Zhang, Particle swarm optimization of tuned mass dampers, *Eng. Struct.* **31**(3) (2009) 715–728.
24. B. Keshtegar and S. Etedali, Nonlinear mathematical modeling and optimum design of tuned mass dampers using adaptive dynamic harmony search algorithm, *Struct. Control Health Monit.* **25**(7) (2018) e2163.
25. Q. Han, X. Zhang, K. Xu and X. Du, Free parameter optimization of DTMDs based on improved hybrid genetic-simulated annealing algorithm, *Int. J. Struct. Stab. Dyn.* **20**(3) (2020) 2050031.
26. S. Etedali, A new modified independent modal space control approach toward control of seismic-excited structures, *Bull. Earthq. Eng.* **15**(10) (2017) 4215–4243.
27. S. Etedali and H. Rakhshani, Optimum design of tuned mass dampers using multi-objective cuckoo search for buildings under seismic excitations, *Alexandria Eng. J.* **57**(4) (2018) 3205–3218.

28. A. Kaveh, S. M. Javadi and R. M. Moghanni, Optimal structural control of tall buildings using tuned mass dampers via chaotic optimization algorithm, *Structures* **28** (2020) 2704–2713.
29. S. Hosseinaei, M. R. Ghasemi and S. Etedali, Optimal design of passive and active control systems in seismic-excited structures using a new modified TLBO, *Period. Polytech. Civ.* **65**(1) (2021) 37–55.
30. S. Q. Moinuddin, S. S. Hameed, A. K. Dewangan, K. R. Kumar and A. S. Kumari, A study on weld defects classification in gas metal arc welding process using machine learning techniques, *Mater. Tod. Proc.* **43** (2021) 623–628.
31. J. Ribeiro, R. Lima, T. Eckhardt and S. Paiva, Robotic Process Automation and Artificial Intelligence in Industry 4.0 — A Literature review, *Procedia Comput. Sci.* **181** (2021) 51–58.
32. P. Jiao and A. H. Alavi, Artificial intelligence in seismology: Advent, performance and future trends, *Geosci. Front.* **11**(3) (2020) 739–744.
33. O. Debauche, S. Mahmoudi, S. A. Mahmoudi, P. Manneback, J. Bindelle and F. Lebeau, Edge computing and artificial intelligence for real-time poultry monitoring, *Procedia Comput. Sci.* **175** (2020) 534–541.
34. H. Wang, Y. Liu, B. Zhou, C. Li, G. Cao, N. Voropai and E. Barakhtenko, Taxonomy research of artificial intelligence for deterministic solar power forecasting, *Energy Convers. Manage.* **214** (2020) 112909.
35. M. Das, S. Sahu and D. R. Parhi, Composite materials and their damage detection using AI techniques for aerospace application: A brief review, *Mater. Tod. Proc.* in press, 2020, doi:10.1016/j.matpr.2020.11.005.
36. L. Li, S. Rong, R. Wang and S. Yu, Recent advances in artificial intelligence and machine learning for nonlinear relationship analysis and process control in drinking water treatment: A review, *Chem. Eng. J.* **405** (2020) 126673.
37. G. Rong, A. Mendez, E. B. Assi, B. Zhao and M. Sawan, Artificial intelligence in healthcare: review and prediction case studies, *Engineering* **6**(3) (2020) 291–301.
38. S. Etedali and N. Mollayi, Cuckoo search-based least squares support vector machine models for optimum tuning of tuned mass dampers, *Int. J. Struct. Stab. Dyn.* **18**(2) (2018) 1850028.
39. M. Yucel, G. Bekdaş, S. M. Nigdeli and S. Sevgen, Estimation of optimum tuned mass damper parameters via machine learning, *J. Build. Eng.* **26** (2019) 100847.
40. Yang, X. S. and S. Deb, Cuckoo search via Lévy flights, *2009 World Congr. Nature and Biologically Inspired Computing (NaBIC)*, Coimbatore, India, 2009, pp. 210–214.
41. X. S. Yang and S. Deb, Multiobjective cuckoo search for design optimization, *Comput. Oper. Res.* **40**(6) (2013) 1616–1624.
42. H. Rakhshani and A. Rahati, Snap-drift cuckoo search: A novel cuckoo search optimization algorithm, *Appl. Soft Comput.* **52** (2017) 771–794.
43. H. Rakhshani, E. Dehghanian and A. Rahati, Hierarchy cuckoo search algorithm for parameter estimation in biological systems, *Chemometr. Intell. Lab. Syst.* **159** (2016) 97–107.
44. X. S. Yang and S. Deb, Cuckoo search: Recent advances and applications, *Neural Comput. Appl.* **24**(1) (2014) 169–174.
45. A. H. Gandomi, S. Talatahari, X. S. Yang and S. Deb, Design optimization of truss structures using cuckoo search algorithm, *Struct. Des. Tall Special Build.* **22**(17) (2013) 1330–1349.
46. A. A. Zamani, S. Tavakoli, S. Etedali and J. Sadeghi, Adaptive fractional order fuzzy proportional–integral–derivative control of smart base-isolated structures equipped with magnetorheological dampers, *J. Intell. Mater. Syst. Struct.* **29**(5) (2018) 830–844.

47. A. A. Zamani, S. Tavakoli, S. Etedali and J. Sadeghi, Online tuning of fractional order fuzzy PID controller in smart seismic isolated structures, *Bull. Earthq. Eng.* **16**(7) (2018) 3153–3170.
48. S. Etedali, K. Hasankhoie and M. R. Sohrabi, Optimal design of pure-friction isolators with and without restoring device: A multi-objective cuckoo search-based approach for seismic-excited structures, *Structures* **25** (2020) 708–719.
49. Z. Yun, Z. Quan, S. Caixin, L. Shaolan, L. Yuming and S. Yang, RBF neural network and ANFIS-based short-term load forecasting approach in real-time price environment, *IEEE Trans. Power Syst.* **23**(3) (2008) 853–858.
50. A. M. Zaki, S. I. Amer and M. Mostafa, Maximum power point tracking for PV system using advanced neural networks technique, *Int. J. Emerg. Technol. Adv. Eng.* **2**(12) (2012) 58–63.
51. W. T. Miller, P. J. Werbos and R. S. Sutton, (eds.), *Neural Networks for Control* (MIT Press, Cambridge, 1995).
52. R. Singh, A. Kainthola and T. N. Singh, Estimation of elastic constant of rocks using an ANFIS approach, *Appl. Soft Comput.* **12**(1) (2012) 40–45.
53. J. Finol, Y. K. Guo and X. D. Jing, A rule based fuzzy model for the prediction of petrophysical rock parameters, *J. Pet. Sci. Eng.* **29**(2) (2001) 97–113.
54. J. S. Jang, Neuro-fuzzy modeling: Architectures, analyses and applications, University of California, Berkeley (1992).
55. T. N. Singh, R. Kanchan, A. K. Verma and K. Saigal, A comparative study of ANN and neuro-fuzzy for the prediction of dynamic constant of rockmass, *J. Earth Syst. Sci.* **114**(1) (2005) 75–86.
56. J. S. Jang, ANFIS: Adaptive-network-based fuzzy inference system, *IEEE Trans. Syst. Man Cybernet.* **23**(3) (1993) 665–685.
57. L. Breiman, Random forests, *Mach. Learn.* **45**(1) (2001) 5–32.
58. K. Florios, I. Contopoulos, G. Tatsis, V. Christofilakis, S. Chronopoulos, C. Repapis and V. Tritakis, Possible earthquake forecasting in a narrow space-time-magnitude window, *Earth Sci. Inf.* **14**(1) (2021) 349–364.
59. S. Moschella, A. Cannata, F. Cannavò, G. Di Grazia, G. Nardone, A. Orasi, M. Picone, M. Ferla and S. Gresta, Insights into microseism sources by array and machine learning techniques: Ionian and Tyrrhenian Sea case of study, *Front. Earth Sci.*, in press, 2020, doi:10.3389/feart.2020.00114.
60. A. P. Singh, D. Vashisth and S. Srivastava, Random forest regressor for layered earth data inversion, in *AGU Fall Meeting 2019* (AGU, 2019), pp. S53D–0483.
61. W. Dubitzky, O. Wolkenhauer, H. Yokota and K. H. Cho, *Encyclopedia of Systems Biology* (Springer Publishing Company, New York, 2013).
62. D. Paper, Scikit-learn regression tuning, *Hands-on Scikit-Learn for Machine Learning Applications* (Apress, Berkeley, CA, 2020), https://doi.org/10.1007/978-1-4842-5373-1_7.